УДК 550.341

ON INCREASE OF EARTHQUAKE CORRELATION LENGTH PRIOR TO LARGE EARTHQUAKES IN CALIFORNIA

I. Zaliapin[1,2], Z. Liu[3], G. Zöller[4], V. Keilis-Borok[1,2,3], D. Turcotte[5]

[1] International Institute of Earthquake Prediction Theory and Mathematical Geophysics, Russian Academy of Sciences, Moscow
[2]Institute of Geophysics and Planetary Physics, UCLA, Los Angeles
[3]Department of Earth and Space Sciences, UCLA, Los Angeles
[4]Institute of Physics and Mathematics, University of Potsdam, Potsdam
[5]Department of Earth and Atmospheric Sciences, Cornell University, Ithaca

It is well established that earthquakes are correlated over distances greatly exceeding their source dimension. Recent studies hypothesize for important associated phenomenon: The area over which earthquake activity is correlated varies in time and might grow prior to a large earthquake. This hypothesis is supported by a wealth of observations, computer simulation, and has theoretical interpretations. Several measures of earthquake correlation lengths were recently suggested by different authors. Here we analyze one of these measures, $\xi(\mathbf{x}, t)$, based on single-link cluster analysis of epicenters. Previous studies have shown the growth of ξ prior to nine large earthquakes in California during 1945-2000. In this paper we study whether the reported growth of the correlation length $\xi(\mathbf{x}, t)$ can be used for earthquake prediction. Our results show that reasonable retrospective prediction of large earthquakes ($M \geq 6.5$) in California can be achieved by using the increase of ξ as a signal for the approach of a large earthquake. Extensive variations of numerical parameters demonstrate the stability of this prediction method. Additionally, we compare the distributions of $\xi(\mathbf{x}, t)$ close and distant in time and space to large earthquakes and find a systematic shift reflecting the increase of the correlation length prior to large earthquakes. Premonitory increases of correlation lengths are seen most clearly in the highly fractured areas near fault junctions. Its predictive power is reduced in more homogeneous regions.

К ВОПРОСУ ОБ УВЕЛИЧЕНИИ РАДИУСА СЕЙСМИЧЕСКОЙ КОРРЕЛЯЦИИ ПЕРЕД СИЛЬНЫМИ ЗЕМЛЕТРЯСЕНИЯМИ В КАЛИФОРНИИ

И. Заляпин[1,2], Ж. Лиу[3], Г. Золлер[4], В. Кейлис-Борок[1,2,3], Д. Туркотт[5]

[1]Международный институт теории прогноза землетрясений и математической геофизики Российской академии наук, Москва
[2]Институт физики Земли и планет, Калифорнийский Университет, Лос-Анджелес
[3]Факультет наук о Земле и космических исследований, Калифорнийский Университет, Лос-Анджелес
[4]Институт физики и математики, Потсдамский Университет, Потсдам
[5]Факультет наук о Земле и атмосфере, Корнельский Университет, Итака

Феномен корреляции землетрясений на расстояниях, намного превосходящих размер их очагов (удаленная сейсмическая корреляция), хорошо известен в геофизике. Недавно была высказана гипотеза о том, что размер области удаленной сейсмической корреляции меняется со временем и может увеличиваться перед сильными землетрясениями. Данная гипотеза подтверждается многочисленными наблюдениями, компьютерным моделированием, и может быть теоретически обоснована. В работе анализируется мера $\xi(t, \mathbf{x})$ радиуса сейсмической корреляции, основанная на кластерном анализе эпицентров землетрясений. Ранее было показано, что $\xi(t, \mathbf{x})$ растет перед сильными событиями в Калифорнии в период 1945–2000 гг. В работе рассмотрен вопрос о возможности алгоритмического прогноза землетрясений на основе указанного роста. Сформулирован алгоритм, примененный для ретроспективного прогноза событий с магнитудой $M \geq 6.5$ в Калифорнии. Качество прогноза оценено с помощью диаграммы ошибок, устойчивость проверена вариацией численых параметров алгоритма. В дополнение, распределение значений $\xi(t, \mathbf{x})$ сопоставлено в областях, близких и удаленных в пространстве–времени от сильных событий. Такой анализ демонстрирует систематическое увеличение радиуса сейсмической корреляции при приближении сильного землетрясения. Предвестниковое увеличение радиуса корреляции наиболее ярко выражено вблизи пересечений основных геологических разломов, в областях, характеризующихся высокой тектонической раздробленностью.

1. Introduction

Earthquakes are correlated over the distances far exceeding their source dimension. Among many manifestations of this phenomenon one observes the simultaneous change of seismicity in large areas [1,2], migration of seismicity along seismic belts [3,4], global interdependence in the occurrence of major earthquakes [5], etc. Ample evidence of long-range correlations comes from the studies of changes in seismic activity prior to large earthquakes [6–13]. There is growing evidence that earthquake correlation ranges are not only large but also increase with time prior to strong earthquakes. Premonitory patterns based on this phenomenon have been recently found in modeled seismicity and in observations [14–20]. Here, we study one specific measure of earthquake correlation range introduced in [18]. Specifically, we focus on the following questions: Can this measure be used for earthquake prediction? If so, how can it be used?

1.1. Premonitory long-range correlations. The area where premonitory patterns can be observed was first estimated by V. Keilis-Borok and L. Malinovskaya [9]. Specifically, it was shown that a) the occurrence rate of moderate-size earthquakes increases years to a decade prior to some large earthquakes, b) the increase, if observed, occurs within a large territory around the approaching earthquake's rupture zone, and c) the size Q of that territory scales with the magnitude M of a large earthquake as

$$\log Q \propto 0.5M. \tag{1}$$

Later studies confirmed these results. Table 1 presents estimates of the linear size of the earthquake preparation area, $R \approx Q^{1/2}$, obtained by differ-

TABLE 1. Estimations of the area where premonitory patterns may be observed

Measure	Year	$R(L)$	Reference
Area of faultbreaks	1964	$\sim 10L$	Keilis-Borok and Malinovskaya, 1964
Distant aftershocks	1975	$10L$	Prozoroff, 1975
Earthquake swarms	1977	$5L - 10L$	Caputo et al., 1977
Bursts of aftershocks, area of faultbreaks, swarms	1980	$5L - 10L$	Keilis-Borok et al., 1980
Algorithm CN*	1983	$5L - 10L$	Keilis-Borok and Rotwain, 1990
Algorithm M8*	1985	$5L - 10L$	Keilis-Borok and Kossobokov, 1990
Algorithm SSE*	1992	$\sim 5L$	Vorobieva, 1999
Number of earthquakes	1995	$\sim 100L$	Press and Allen, 1995
Number of earthquakes	1996	$\sim 5L$	Knopoff et al., 1996
Benioff strain release	1989	$\sim 5L$	Varnes, 1989 Bowman et al., 1998 Jaume and Sykes, 1999
Near-simultaneous pairs of earthquakes	2001	$\sim 3L$	Shebalin et al., 2000
Correlation length via Single Link Cluster	2001	$\sim 5L$	Zoller et al., 2001 Zoller and Hainzl, 2001
Simultaneous activization of fault branches	2002	$\sim 10L$	Zaliapin et al., 2002

* References are given to later comprehensive reviews; not to original work.

ent authors; to make results comparable they are given as relations between R and the linear dimension L of the coming earthquake. One can see surprisingly good agreement despite the diversity of applied approaches, data, and regions considered. V. Keilis-Borok and L. Malinovskaya [9] studied the total area of faultbreaks and demonstrated its increase prior to some large earthquakes; A. Prozorov [10] observed that the location of future large earthquake might be depicted years in advance by "distant aftershocks": earthquakes that immediately follow a mainshock at distances 10 times larger than its linear source dimension; study [21] showed that swarms of earthquakes of medium magnitude might occur years prior to large earthquakes. In the wake of these findings the family of algorithmically defined intermediate-term earthquake premonitory seismicity patterns was introduced and tested worldwide during the last 20 years. The latest comprehensive reviews can be found in [12, 22]. These patterns reflect the following changes of seismic-

ity: increase of earthquake activity, clustering, transformations of magnitude distribution (Gutenberg-Richter law), and increase of earthquake correlation range. They have been jointly used in the earthquake prediction algorithms M8 [23], CN [24] and SSE [25]. These algorithms are validated by well-documented advance predictions [12,25,26,27]. Importantly, the relation (1) is used to renormalize the prediction algorithms for different target magnitudes M. During the past decade, large attention was given to study accelerating seismic moment release prior to large and great earthquakes [13,28,29,30]. Relation (1) was shown to describe the size of the area where seismic activity accelerates prior to a large earthquake. Recently, F.Press and C. Allen extended the frontiers of the long-range-correlation paradigm by demonstrating that "earthquakes in southern California occur within a larger system that includes at least the Great Basin and the Gulf of California" [5]. Particularly, they argue that an earthquake predicted for Parkfield is not likely to occur until activity picks up in one of those distant areas.

Long-range earthquake correlations are observed in modeling [14,17,31–34] and explained in the framework of "self-organized criticality", "critical point behavior", and "finite-time singularity" concepts that have reinforced each other during the last decade [35–42].

1.2. Premonitory increase of earthquake correlation length. Recent studies hypothesize for important associated phenomena: the area over which earthquake activity is correlated varies in time and might grow prior to a large earthquake. Several explicitly defined measures for the earthquake correlation range were introduced and studied.

Pepke et al. [14] considered a measure AZS (Active Zone Size) for a dynamical model of a fault; it was demonstrated that AZS has a much stronger predictive power comparing to seismic activation and fluctuations of activity in predicting synthetic earthquakes. V.Kossobokov and J.Carlson [15] demonstrated that by using AZS instead of seismic activity in the earthquake prediction algorithm M8 [23], one improves its performance for western United States.

The study of the colliding cascade model of seismicity introduced two earthquake correlation measures: Accord and ROC (Radius of Correlation) [17,34]. The measure Accord accounts for the geometry of a regional fault network. Its predictive power for observed seismicity of southern California was demonstrated in [20]. Short-term premonitory increases of the measure ROC was found in [16] for observed seismicity of Lesser Antilles.

Study [18] introduced the correlation length measure $\xi(\mathbf{x}, t)$ based on single-link cluster analyses of epicenters. The $\xi(\mathbf{x}, t)$ was evaluated for epicenters $\mathbf{x}_i$ of nine large earthquakes in California for the period preceding each event. It was shown that $\xi(\mathbf{x}_i, t)$ increases in time prior to each of

the earthquakes considered; the increase lasting for periods from years to decades. In this paper we consider how this measure can be used for earthquake prediction.

1.3. Verifying premonitory phenomenon. Is the increase of $\xi(\mathbf{x}, t)$ observed in [18] a distinctive feature of the area around and the time preceding a large earthquake? More explicitly, can one use the increase of $\xi(\mathbf{x}, t)$ to predict a large earthquake? Answering this question on the sole basis of observations preceding large earthquakes can be questioned: a trivial analogue is an attempt to predict large earthquakes by the advent of a New Year. It is of course true that one witnesses a New Years celebration a year prior to *any* large earthquake; at the same time a large earthquake cannot be *predicted* this way.

We consider the correlation length $\xi(\mathbf{x}, t)$ introduced in [18] for California during 1945–2000; it is evaluated over a spatially uniform grid that covers the whole territory. First, we analyze spatio-temporal distributions of ξ values within areas close and distant in time and space to large ($M \geq 6.5$) earthquakes. Second, we perform a retrospective prediction using the increase of $\xi(\mathbf{x}, t)$ as a signal of an approaching large earthquake. Quality and stability of the prediction are evaluated. The data and definition of the correlation length are taken unchanged from [18].

2. Data

We analyze seismicity of California in the latitude range 32°N–40°N and longitude range 114°W–125°W within the period 1945–2000. The data are taken from Worldwide Earthquake Catalog produced by The Council of the National Seismic System (CNSS) (available at http://quake.geo.berkeley.edu/cnss). Only earthquakes with magnitudes $M \geq 4.0$ are kept for analysis; aftershocks are not excluded. As a result, 3322 earthquakes are considered. Nine of them have magnitude $M \geq 6.5$; they are listed in Table 2 and shown in Fig. 1.

3. Correlation length

The correlation length $\xi(\mathbf{x}, t)$ is defined as the median of the length distribution of links, which form a single-link cluster for epicenters of consecutive K earthquakes occurred prior to the time t and within a circle of radius R centered at the point $\mathbf{x}$ [18]. The procedure for constructing a single-link cluster connecting M points in a metric space is the following [43]: 1) Each point of M is connected with its nearest neighbor; $M_1 < M$ clusters are pro-

TABLE 2. Large earthquakes considered

	Date	M	Longitude, °W	Latitude, °N	Area
a	July 21, 1952	7.5	119.02	35.00	Kern County
b	April 9, 1968	6.5	116.13	33.19	Borrego Mountain
c	February 9, 1971	6.6	118.40	34.41	San Fernando
d	May 2, 1983	6.7	120.32	36.22	Coalinga
e	November 24, 1987	6.6	115.84	33.01	Superstition Hills
f	October 18, 1989	7.0	121.88	37.04	Loma Prieta
g	June 28, 1992	7.3	116.44	34.20	Landers
h	January 17, 1994	6.6	118.54	34.21	Northridge
i	October 16, 1999	7.1	116.27	34.59	Hector Mine

Fig. 1. Earthquakes with $M \geq 6.5$ since 1952 in California: circle (a) Kern County, 1952, $M = 7.5$; (b) Borrego Mountain, 1968, $M = 6.5$; (c) San Fernando, 1971, $M = 6.6$; (d) Coalinga, 1983, $M = 6.7$; (e) Superstition Hills, 1987, $M = 6.6$; (f) Loma Prieta, 1989, $M = 7.0$; (g) Landers, 1992, $M = 7.3$; (h) Northridge, 1994, $M = 6.6$; (i) Hector Mine, 1999, $M = 7.1$. After [18]

duced; 2) Each cluster of M_1 is connected with its nearest neighbor; distance between clusters is a minimum distance between points from these clusters; $M_2 < M_1 < M$ clusters are produced; 3) This procedure is repeated until all points are connected within a single cluster.

The analysis was carried out by considering a spatial grid G with cell size of $0.5° \times 0.5°$. The correlation length $\xi(\mathbf{x}, t)$ was calculated at each of 247 nodes of the grid for the time period 1945–2000. It was calculated at each node with different sliding event window size K and circle radii R: K was varied from 15 to 25 with step 2; R was varied from 100 km to 600 km with step 100 km; therefore 36 versions of the correlation length were calculated for each spatial location. Only those circles that contain more than 100 earthquakes during the whole time period are left for further analysis. It is worth mentioning that on average the event window of size $K = 15$ corresponds to 0.97 yr, $K = 25$ to 1.51 yr.

The function $\xi(\mathbf{x}, t)$ for the location $\mathbf{x} = (34°\text{N}, 116.5°\text{W})$, close to the epicenter of Landers earthquake (1992, $M = 7.3$), is shown in Fig. 2.

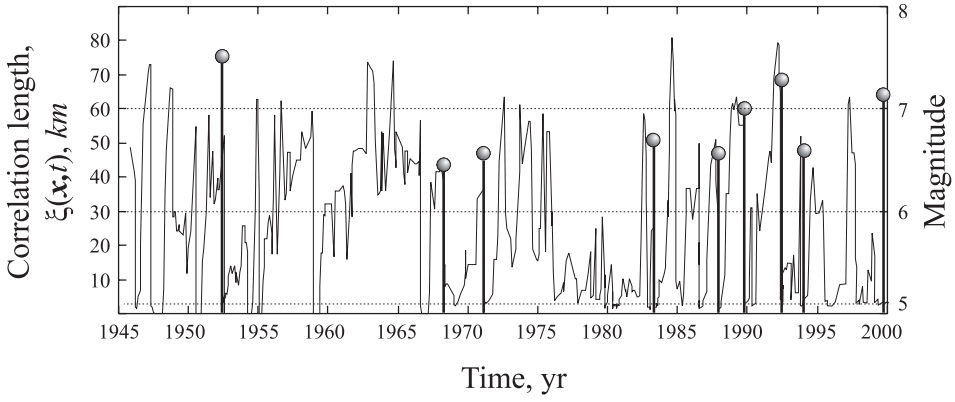

Fig. 2. Typical correlation length $\xi(\mathbf{x}, t)$ evaluated for the location $x = (34°\text{N}, 116.5°\text{W})$, close to the epicenter of Landers earthquake (1992, $M = 7.3$). Vertical lines mark occurrence times of large earthquakes. See discussion in Sect. 3

It corresponds to $K = 25$, $R = 600$ km; vertical lines mark the occurrence time of large ($M \geq 6.5$) earthquakes. There is a sharp increase of the correlation length during 2 years prior to Landers; at the same time the general behavior of the function $\xi(\mathbf{x}, t)$ is quite irregular and unstable. One observes large spikes over the whole time period; not necessarily preceding a large earthquake. Clearly, this single function does not say too much about large earthquake occurrence. However, what is of interest is to study the collective behavior of $\xi(\mathbf{x}, t)$ at different spatial locations to check whether its high values can be observed more often prior to a large earthquake.

4. Distribution analysis

In this section we analyze the distributions of ξ values for two distinct spatio-temporal zones: 1) close in time and space to epicenters of large earthquakes and 2) distant in time and space from the epicenters of large earthquakes. The first zone is called *zone* **D**, for *dangerous*; the second zone is called *zone* **N**, for *non-dangerous*. Ideally, one should observe premonitory phenomena within zone **D**, and should not within zone **N**. This simple and straightforward analysis is well known in pattern recognition and was used successfully in many geophysical studies.

Let $(\mathbf{X}_i, T_i), i = 1, \ldots, n_{eq}$ be space and time coordinates of n_{eq} large earthquakes, which occurred within the analyzed time-space volume. Following are the definitions of zones **A**, **D**, and **N** used in the distribution analyses. Qualitatively, a spatio-temporal point belongs to zone **A** (**D**) if it is close in space and time to one of the large earthquakes and lies after it (prior to it) in time. Formally, point $(\mathbf{x}, t)$ belongs to zone **A** if and only if the following two conditions hold for at least one index k, $1 \le k \le n_{eq}$: 1) $|\mathbf{X}_k - \mathbf{x}| < r_A$; 2) $0 < t - T_k < T_A$. Here $|\cdot|$ denotes a spherical distance. Point $(\mathbf{x}, t)$ belongs to zone **D** if and only if it does not belong to zone **A** and the following two conditions hold for at least one index k: 1) $|\mathbf{X}_k - x| < r_{\mathbf{D}}$; 2) $0 < T_k - t < T_{\mathbf{D}}$. Point $(\mathbf{x}, t)$ belongs to zone **N** if and only if it does belong neither to zone **A** nor zone **D**. $r_A, T_A, r_{\mathbf{D}}$, and $T_{\mathbf{D}}$ are numerical parameters. Note that each spatio-temporal point belongs to one and only one of zones **A**, bf D, and **N**.

Zone **A** covers the aftermath of a large earthquake; points from this zone are excluded from the analysis. Thus, only the ξ values evaluated within zones **D** and **N** are considered. This is especially important in our case when aftershocks are not eliminated and dramatically affect the dynamics of the correlation length $\xi(\mathbf{x}, t)$. Figures 3a,b show distributions $H_{\mathbf{D}}$ and $H_{\mathbf{N}}$ of the correlation length $\xi(\mathbf{x}, t)$ within zones **D** and **N** respectively; parameters used to construct the distributions are indicated in bold in the first column of Table 3. These distributions are coarsely estimated at three bins each containing 1/3 of the correlation length values observed within zones **D** and **N** together. Clearly, one observes a discrepancy: the distribution $H_{\mathbf{N}}$ is almost uniform while the distribution $H_{\mathbf{D}}$ favors high values of the correlation length. To further illustrate this observation we consider the difference of the distributions: $H_\Delta = H_{\mathbf{D}} - H_{\mathbf{N}}$, which is shown in Fig. 3 c. Positive values of this difference for the right bin, H_Δ ("high"), indicate that high values of the correlation length are observed more often within zone **D**.

Panels d-f of Fig. 3 illustrate the distribution analysis with parameters listed in the third column of Table 3. The qualitative picture is the same

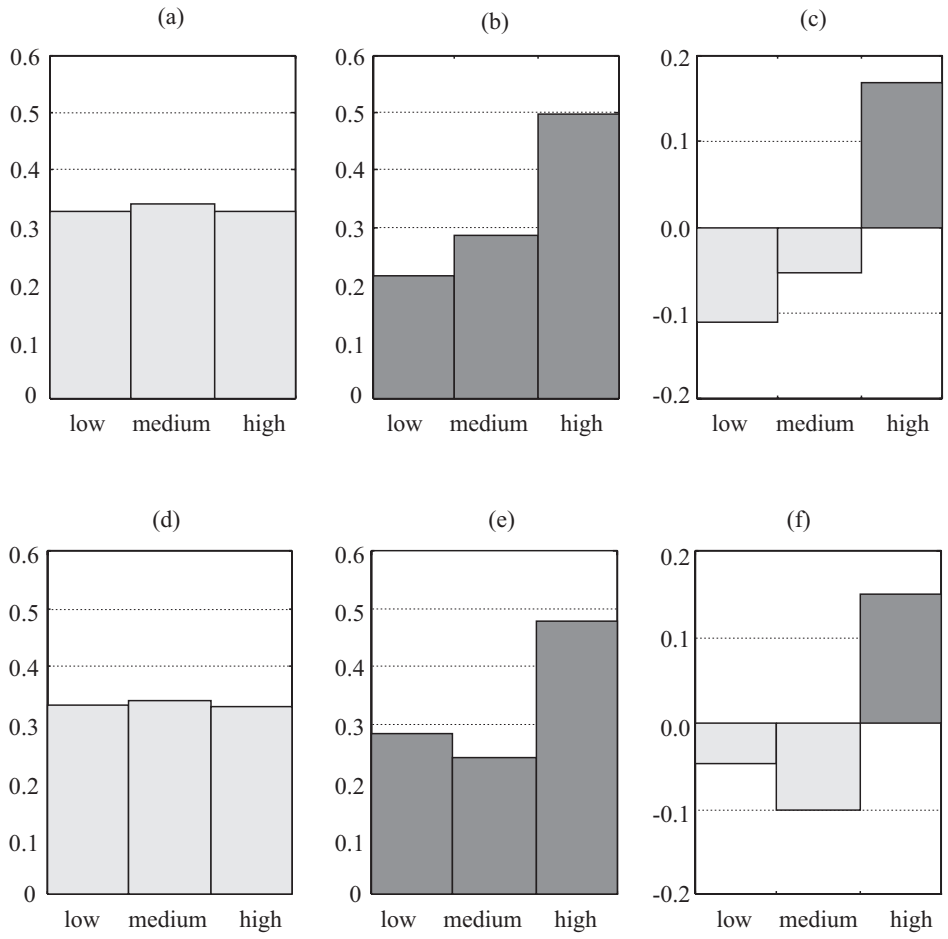

Fig. 3. Distribution analysis. Distribution of ξ is coarsely evaluated at three bins, "low", "medium" and "high", each containing 1/3 of values considered. Panels (a)–(c) correspond to parameters given in the first column of Table 3, (d)–(f) to parameters given in the third column. (a), (d) distribution H_N within zone **N**, distant in time and space from large earthquakes; (b), (e) distribution H_D within zone **D**, close in time and space to large earthquakes; (c), (f) difference of distributions, $H_\Delta = H_D - H_N$. Note the discrepancy of distributions H_N and H_D: there is a clear shift toward high values within zone **D**, which is depicted by positive values of the difference H_Δ("high")

TABLE 3. Distribution analysis (Sect. 4). Other parameters are fixed: $K = 25$, $r_A = r_D = 100$km, $T_A = 2$ yr

R, km	600*	600	500	500	400	400	300	300	200	200	100	100
T_D, yr	1	5	1	5	1	5	1	5	1	5	1	5
H_Δ("high"), %	16	5	15	6	13	5	6	1	4	7	-3	7

*Sets of parameters given in bold are discussed in the text (Sect. 4) and illustrated in Fig. 3

as in panels a-c: there is a shift of the distribution toward high values within zone **D**. Results for different parameter values are collected in Table 3. Due to qualitative similarity of analyzed distributions and the obvious relation H_Δ("low") $+H_\Delta$("medium") $+H_\Delta$("high")$= 0$, only the differences H_Δ("high") (in %) are shown. The results presented in the table demonstrate that the distribution shift is stable under variations of parameters.

Being calculated with $T_{\mathbf{D}} = 1$ yr, H_Δ("high") decreases with the radius R from 16% to 5%; it remains nearly 5% for $T_{\mathbf{D}} = 5$ yr, i.e., the best statistical separation of zones **D** and **N** are possible within an extended territory, $R = 600$ km, during the relatively short time period of 1 year; it became worse for improperly long times or small territories.

While the discrepancy between the distributions $H_{\mathbf{D}}$ and $H_{\mathbf{N}}$ is evident, it is in fact not too large. The maximum difference between distributions reported in Table 3 is only 16%. Is it enough to distinguish zones **D** and **N** in practice? Is the correlation length a reliable signal of a large earthquake approach? To answer these questions, we analyze retrospective prediction that could be done using the correlation length as a precursor of a large earthquake.

5. Retrospective prediction

In this section we consider retrospective predictions targeted at nine large ($M \geq 6.5$) earthquakes in California during 1945–2000; they are listed in Table 2. The predictions are based on the increase of the correlation length defined in Sect. 3.

The prediction methodology that we use here is based on pattern recognition analyses of infrequent events introduced to geophysics by I. M. Gelfand in the early 70-s [44]; it was successfully used for many years in the quest for premonitory seismicity patterns (see review in [12, 22]). The major trait of this approach is its robustness: results are coarse but stable. Prediction is of the yes-no type: we declare precisely outlined alarms and count all successes and errors. Exhaustive variation of the prediction's adjustable elements evaluates its quality and stability. A pivotal tool for such an evaluation is the *error diagram* (Sect. 5.2), which sums up different errors of prediction, allows the comparison of different prediction methods and optimization of prediction strategies. The error diagram was introduced to seismological studies by G. Molchan [45] and became an indispensable tool in earthquake prediction research.

5.1. Scheme of analysis. The function $\xi(\mathbf{x}, t)$ is monitored at each node $\mathbf{x}_i$ of the grid G. Once it exceeds the threshold C_i an *individual alarm* is declared for the time Δ within the circle of radius r centered at $\mathbf{x}_i$. Threshold

C_i is defined as Q-percentile of values $\xi(\mathbf{x}_i, t)$ observed at the location $\mathbf{x}_i$. An *alarm cluster* is defined as a union of alarms that are connected in space and time. This means that two alarms belong to the same cluster if and only if there is a spatio-temporal path, which connects these alarms and is totally covered by these and other alarms (obviously, all alarms that cover this path also belong to the same cluster). If a target earthquake happens to be covered by an alarm cluster it is called a *predicted earthquake*; otherwise it is called an *unpredicted earthquake*. An alarm cluster that covers at least one of the target earthquakes is called a *successful alarm*; otherwise it is called a *false alarm*. Note that the definition of predicted/unpredicted earthquakes would not change if one considered individual alarms instead of alarm clusters; and this is not the case for successful/false alarms.

5.2. Error diagrams. Suppose that the prediction was performed during the time interval of length T (yr) within the area of S (km^2) and N large earthquakes occurred within this period; A alarm clusters were declared and A_f of them are false; all the alarms altogether cover the spatio-temporal volume V_A (yr $\times$ km^2); N_f target earthquakes were unpredicted. Prediction is described by the following dimensionless errors: the fraction of unpredicted earthquakes, $n = N_f/N$; the relative alarm coverage, $\tau = V_A/(T \times S)$; the fraction of false alarms, $f = A_f/A$.

The *error diagram* sums up the prediction errors; each particular prediction corresponds to a single point in (n, τ, f) space. The error diagram will be used to evaluate the predictive power of our prediction algorithm and its stability.

The evaluation of the correlation length $\xi(\mathbf{x}, t)$ involves two numerical parameters, event window size K and data collection radius R; a prediction with a particular function ξ depends on another three parameters, threshold quantile Q, alarm radius r, and alarm duration Δ. Each combination of these five parameters corresponds to a separate prediction, characterized by three errors: $n(K, R, Q, r, \Delta)$, $\tau(K, R, Q, r, \Delta)$, $f(K, R, Q, r, \Delta)$.

5.3. Prediction. We performed predictions following the scheme of Sect. 5.1. The parameters are varied as follows: $K = 15, 17, \ldots, 25$; $R = 100, 200, \ldots, 600$ km; $Q = 0.5, 0.6, 0.7, 0.8, 0.9, 0.95, 0.99$; $\Delta = 0.5, 1, \ldots, 10$ yr; r was always fixed at 100 km. Over 5,000 predictions were considered altogether.

An error diagram for predictions with $R = r = 100$ km is shown in Fig. 4; it brings together 840 individual predictions with different values of parameters K, Q, and Δ. The fact that the fraction of space-time alarm duration is always greater than 15% is due to our prediction scheme. Each node is forced to declare at least one alarm; thus the total space-time area covered by alarms cannot be arbitrary small even for the highest values of

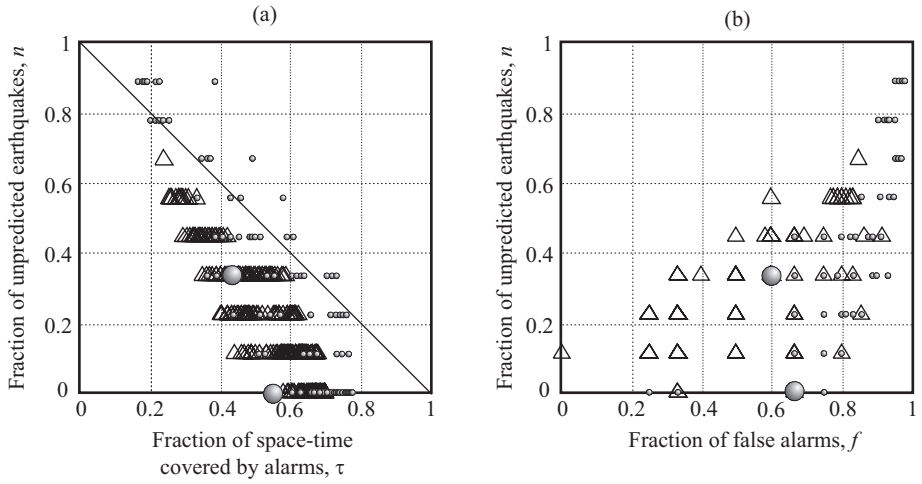

Fig. 4. Error diagram for retrospective prediction in California during 1945–2000. Each point corresponds to a fixed set of parameter values. (a) Fraction of space-time covered by alarms, τ, vs. fraction of failures to predict, n. (b) Fraction of false alarms, f, vs. fraction of failures to predict, n. Parameters are varied as follows: $K = 15, 17, \ldots, 25$; $R = r = 100$ km; $Q = 0.5, 0.6, 0.7, 0.8, 0.9, 0.95, 0.99$; $\Delta = 0.5, 1, \ldots, 10$ years. Triangles correspond to a narrowed range of parameters: $Q \geq 0.9, \Delta \geq 2$ years. Large circles mark two versions of predictions that are used for the stability analysis (Sect. 5.4, Fig. 6) and in the analysis of individual predictions (Sect. 5.5, Fig. 7). Diagonal line in panel (a) correspond to a random binomial prediction: alarm is declared at each time with probability $p = \tau$, and is not declared with probability $1 - p = 1 - \tau$; deviations from the diagonal line depict predictive power of a precursor [45]

the threshold Q. Notably, the $n - \tau$ part of the error diagram is asymmetric relative to the diagonal line of random prediction and most of the points are distanced from this line; thus indicating the predictive power of the considered precursor. Still, some points lie above the diagonal line, implying a prediction worse than "random". Is it an inherent drawback of prediction by the correlation length $\xi(\mathbf{x}, t)$? In fact, we have considered such a broad range of parameter values that it would be too naive to hope that all of them will produce reasonable result. Triangles in Figure 4 mark predictions obtained within the narrowed parameter range: $Q \geq 0.9, \Delta \geq 2$ yr. All these points are nicely clustered and separated from the random prediction line; the number of false alarms decreases.

Previous studies suggest that premonitory phenomena scale with the size of approaching earthquake. Thus it is natural to expect that the increase of the correlation length should be observed within different spatio-temporal zones for earthquakes of different magnitude. Figure 5 shows separate error diagrams for predictions targeted at earthquakes of magnitude $M \leq 7.0$ and $M > 7.0$ (Kern County, Landers, Hector Mine). Panels a, and b correspond to $M \leq 7.0$, $R = r = 100$ km, $Q \geq 0.9$, $\Delta \geq 2$ yr; panels c, and d to $M > 7.0$, $R = 200$, $r = 100$ km, $Q \geq 0.95$, $\Delta \leq 5$ yr. Points on both error

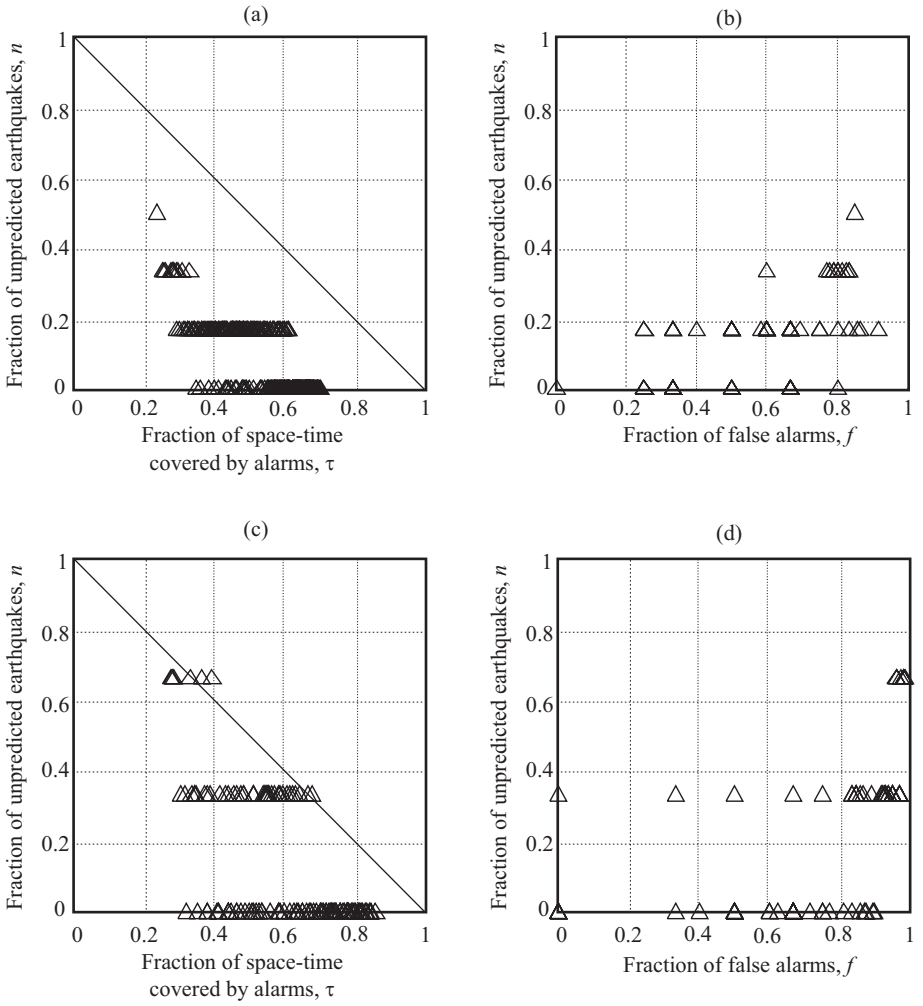

Fig. 5. Error diagrams for predictions of different target magnitudes. (a), (b) $M \leq 7.0$, $K = 15, 17, \ldots, 25$, $R = r = 100$ km, $Q \geq 0.9$, $\Delta \geq 2$ yr; (c), (d) $M > 7.0$, $K = 15, 17, \ldots, 25$, $R = 200, r = 100$ km, $Q \geq 0.95$, $\Delta \leq 5$ yr. See details in Sect. 5.3

diagrams in Fig. 5 lie closer to the origin, $n = \tau = f = 0$, than points in Fig. 4, which means that prediction quality has improved. Noteworthy is the difference in parameters corresponding to the improved predictions. Prediction of earthquakes with $M > 7.0$ is better with $\xi(\mathbf{x}, t)$ estimated within an area of $R = 200$ km; prediction $M \leq 7.0$ is better with $\xi(\mathbf{x}, t)$ estimated within a smaller area, $R = 100$ km. Predictions of $M > 7.0$ are more precise: The correlation length increases less than 5 years prior to a target earthquake; while for $M \leq 7.0$ the increase is observed 2–10 years in advance.

5.4. Stability of prediction. In the previous section we demonstrated that there is a wide domain of parameters that produce reasonable predictions. But how stable are these predictions? How does a slight variation of parameters affect the prediction outcomes? To answer these questions we single out two predictions marked by large open circles in Fig. 4, slightly change values of numerical parameters corresponding to these versions, and compare our results on the error diagram (Fig. 6).

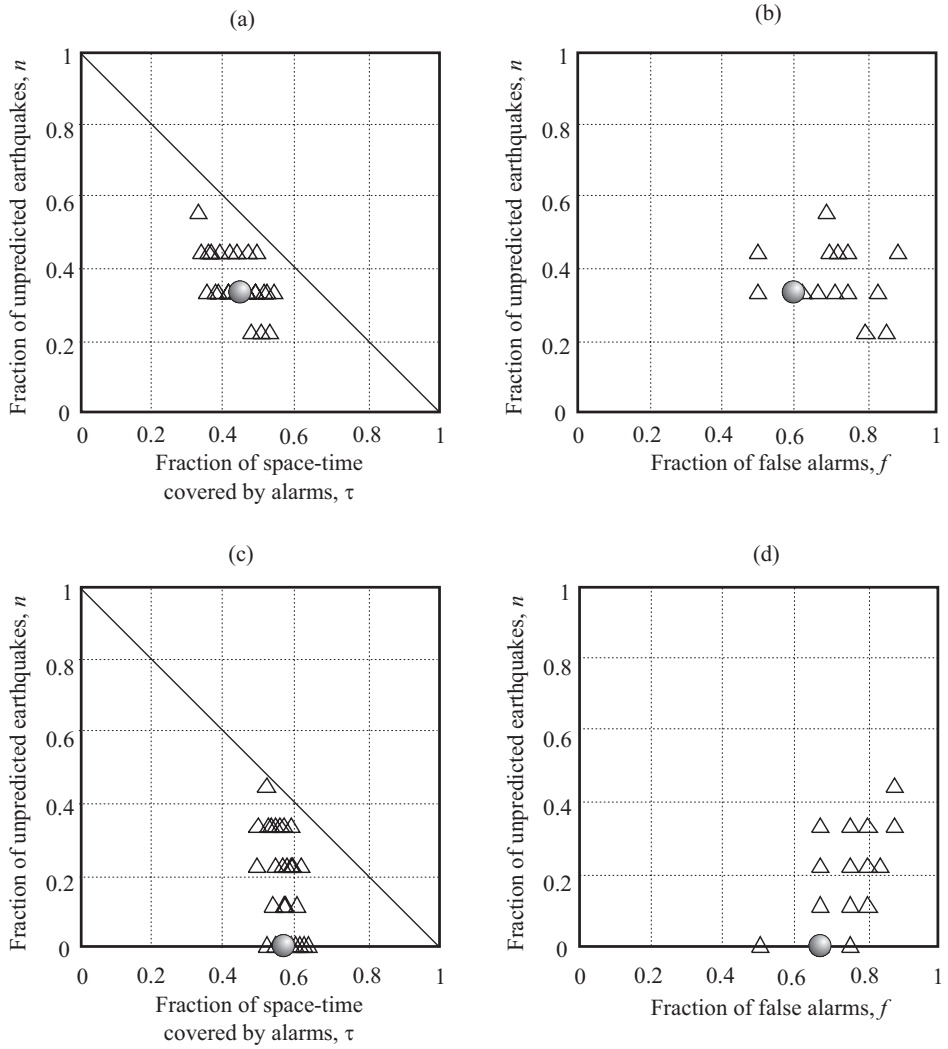

Fig. 6. Stability analysis: a particular version of prediction is considered, parameters of this prediction are slightly varied, and results corresponding to these variations are shown in the error diagram. Filled circles: original versions of prediction, triangles – variations. Two versions of prediction are considered: $K = 25$, $R = r = 100$ km, $Q = 0.95$, $\Delta = 2$ yr (panels (a), (b)), and $K = 19$, $R = r = 100$ km, $Q = 0.9$, $\Delta = 1$ yr (panels (c), (d)). These two versions of prediction are marked by large circles at error diagram in Fig. 4

Parameter values and their variations are given in Table 4. The first row of the table corresponds to panels a, b, and the second to panels c, d.

TABLE 4. Parameters for stability test (Sect. 5.4)

R, km	K	Q	r, km	Δ, years
100	21, 23, **25**	0.9, **0.95**, 0.99	**100**	1.5, **2**, 2.5
100	17, **19**, 21	0.8, **0.9**, 0.95	**100**	0.5, **1**, 1.5

Stability of prediction is depicted by the clustering of points with regard to the original version of prediction. Obviously, stability is high in panels a, b; and is slightly worse in panels c, d. This is due to our choice of versions for our stability analysis. The original prediction for panels a, b is taken from the center of the point cluster on the error diagram (Fig. 4); as a result it gives not the best but stable and reproducible predictions. On the contrary, the original prediction for panels c, d is taken from the boundary of the cluster. It produces better-than-average but less stable results. Generally, the "best" versions of prediction, taken from the border of the error diagram cluster, outline boundaries of the predictive power of a given method rather than reflect the realistic quality of prediction.

So far we have considered averaged statistics of prediction. Next we focus on individual predictions for specific spatial locations.

5.5. Individual predictions. At any given time a particular spatial point may be covered by more than one individual alarm, because an alarm produced at spatial point $\mathbf{x}$ is declared not only for this point but for an extended circle centered at $\mathbf{x}$. In this section we consider the number of alarms that cover a particular spatial location at a given time moment. We focus our attention on three locations: epicenters of Borrego Mountain (1968, $M = 6.5$), San Fernando (1971, $M = 6.6$) and Landers (1999, $M = 7.3$) earthquakes. The number of alarms declared for each of these locations is shown in Fig. 7a. Predictions are made with parameters shown in bold in the first row of Table 4. The top panel corresponds to the Borrego Mountain epicenter, the middle to San Fernando, and the bottom to Landers. Vertical lines mark the occurrence times of these earthquakes. In each panel we additionally show the occurrence times of earthquakes that were within 100 km from the location considered. Thus, we also show Superstition Hills (1988, $M = 6.6$) earthquake in the top panel, Kern County (1952, $M = 7.5$) and Northridge (1994, $M = 6.6$) in the middle panel, and Hector Mine (1999, $M = 7.1$) in the bottom panel. Predictions for the same three locations but with different parameter values are shown in Fig. 7 b; parameters are given in bold in the second row of Table 4.

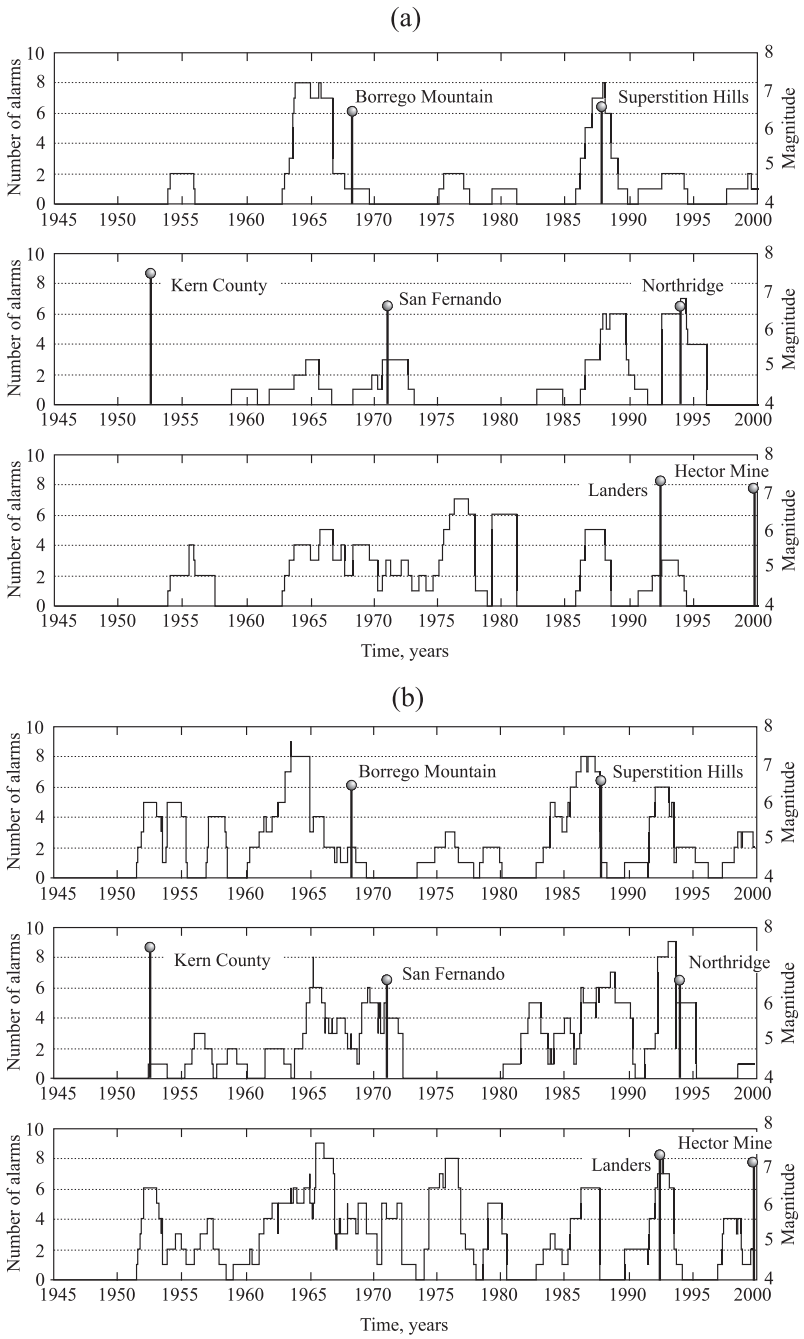

Fig. 7. Number of alarms that cover a particular spatial location at time t. Vertical lines mark occurrence times of large earthquakes that fell within 100 km from the location considered. Top panel corresponds to the epicenters of Borrego Mountain earthquake (1968, $M = 6.5$), middle to San Fernando (1971, $M = 6.6$) and bottom to Landers (1999, $M = 7.3$). (a) $K = 25$, $R = r = 100$ km, $Q = 0.95$, $\Delta = 2$ yr, (b) $K = 19$, $R = r = 100$ km, $Q = 0.9$, $\Delta = 1$ yr. These two versions of prediction are marked by large circles in the error diagram in Fig. 4

Figures 7 a, b give a typical picture of what happens within the regions considered. Prediction works reasonably for Imperial Valley earthquakes (top panel) and in the area near the San Andreas – Garlock triple junction (middle panel); increases of the correlation length are definitely associated with times preceding large earthquakes. At the same time the prediction fails when it is shifted to the Mojave Desert where a pronounced increase of the correlation length occurred in 1970s but faded away by 1990s when the two largest earthquakes occurred.

Similar analysis shows that Loma Prieta earthquake (1989, $M = 7.0$) is usually predicted with a couple of false alarms within its territory. The Coalinga earthquake (1983, $M = 6.7$) is typically missed. The correlation length significantly increases within its territory only in the late 1990s; 10 years after the event. A notable feature in Fig. 7 is the pronounced clustering of alarms in time.

6. Discussion and conclusions

1. We have examined the hypothesis that the earthquake correlation length increases prior to large earthquakes in California and may be used for earthquake prediction. With this aim in view, we analyzed the measure $\xi(\mathbf{x}, t)$ of correlation length introduced in [18]. First, we considered statistical distribution of the values of the correlation length $\xi(\mathbf{x}, t)$ and found the shift toward high values within the areas close in space and time to a large earthquake. Second, we performed retrospective predictions of large earthquakes in California during the period 1945–2000, evaluated its performance and found the set of parameters that gave reasonable and stable prediction quality. Finally, we analyzed predictions for territories around epicenters of large earthquakes.

2. Our results imply that the measure $\xi(\mathbf{x}, t)$ does increase prior to a large earthquake within an extended region around the ensuing epicenter. Importantly, we were able to observe that phenomenon using the *same* fixed set of parameters for *the whole* space and time considered. Moreover, we outlined a large domain of parameters that can be used to reproduce the general result.

3. At the same time, the premonitory increase of the correlation length is weak; e.g. distributions of ξ values for zones **D** and **N** differ by less than 20% only. This situation is usual for prediction research; it is well known that individual premonitory patterns typically perform not so well and should be considered together within a complex prediction algorithm. This is the case for well-tested prediction algorithms M8, CN, and SSE. Our results suggest that the increase of earthquake correlation range can be considered as a reliable individual precursor.

4. From results in Sect. 4 and 5 we conclude that the best statistical discrimination of zones **D** and **N** corresponds to using a large territory ($R = 600$ km) to evaluate the correlation length. On the contrary, the best prediction corresponds to a smaller territory, $R \leq 200$ km. This is caused by a large number of "false" increases of the correlation length evaluated within the large circles. While high values of ξ are definitely observed prior to large earthquakes (see Fig. 2); they are also frequently seen elsewhere. The number of "false" high values is small enough not to destroy statistics (Sect. 4), but is unacceptable to construct reasonable prediction. This provides a good illustration why statistical difference is not equivalent to the possibility of prediction. Furthermore, this explains why the analysis of only times and spaces around large earthquake (zones **D**) is insufficient to make conclusions about the predictive power of a phenomenon.

5. Results of Sect. 5.5 imply that premonitory increases of the correlation length are best observed for the Imperial Valley and for the area around the San Andreas – Garlock junction. It is not very clear in the Mojave Desert, and along the northern San Andreas fault. These observations suggest a hypothesis that the increase of the correlation length is a phenomenon characteristic for highly fractured regions comprising diverse faults and/or fault systems. Clearly, this hypothesis needs further systematic analysis and cannot be tested by data and methods considered in this paper.

6. Alarms produced by increased correlation length clearly tend to cluster in space and time. It is worth further study to explore how this clustering may be used to improve prediction. Particularly, results of Sect. 5.5 suggest that prediction can be significantly improved using the number of alarms declared for a given spatial point as a precursor.

7. The definition of the earthquake correlation length used in this paper is debatable. The function $\xi(\mathbf{x}, t)$ does reflect a multitude of seismicity features not necessarily connected with the studied phenomenon. Most obviously, it decreases due to aftershocks and swarms (see Fig. 2). Nevertheless, it demonstrates stable predictive power (Sect. 5.3, 5.4) and allows distinguishing between space and time close and distant from a large earthquake (Sect. 4). Further investigations of the earthquake correlation length dynamics seem promising to improve its definition and explore potential predictive power.

8. The measure ξ reflects specific features of earthquake clustering depicted by single-link clusters. Noteworthy is an alternative approach to quantitative analysis of premonitory seismicity clustering that was developed by A. Blanter and M. Shnirman in [46] and recently extended to the prediction in a sand-pile model by A. Shapoval and M. Shnirman in [47].

Acknowledgements. The authors sincerely thank V. Pisarenko, G. Molchan and B. Naimark for valuable comments and suggestions. We gratefully acknowledge the financial support from *The 21st Century Collaborative Activity Award for Studying Complex Systems* (James McDonnell Foundation); INTAS, grant 99-00099; and the Deutsche Forschungsgemeinschaft (SFB 555).

REFERENCES

1. *Mogi K.* Earthquake prediction. Tokyo: Academic Press, 1985.
2. *Press F., Allen C.* Patterns of seismic release in the southern California region // J. Geophys. Res. 1995. Vol.100, N 4. P.6421–6430.
3. *Richter C.F.* Elementary seismology. San Francisco: W.H. Freeman and Co. 1958.
4. *Mogi K.* Migration of seismic activity // Bull. Earthq. Res. Inst., Tokyo Univ. 1968. Vol.46. P.53–74.
5. *Romanowicz B.* Spatiotemporal patterns in the energy-release of great earthquakes // Science. 1993. Vol.260. P.1923–1926.
6. *Willis B.* Earthquake risk in California 8 earthquake districts // Bull. Seism. Soc. Amer. 1924. Vol.14. P.9–25.
7. *Imamura A.* Theoretical and applied seismology. Tokyo: Maruzen, 1937.
8. *Gutenberg B., Richter C.F.* Seismicity of the Earth and associated phenomena. N.Y.: Hafner. 1954.
9. *Keilis-Borok V.I., Malinovskaya L.N.* One regularity in the occurrence of strong earthquakes // J. Geoph. Res. 1964. Vol.69. P.3019–3024.
10. *Прозоров А.Г.* Изменения сейсмической активности, приуроченные к сильным землетрясениям // Интерпретация данных сейсмологии и неотектоники. М.: Наука, 1975. С.71–72. (Вычисл. сейсмология; Вып.8).
11. *Shaw B.E., Carlson J.M, Langer J.S.* Patterns of seismic activity preceding large earthquakes // J. Geophys. Res. 1997. Vol.97. P.479.
12. *Keilis-Borok V.I., Shebalin P.N. Eds.* Dynamics of lithosphere and earthquake prediction // Phys. Earth Planet. Inter., Special Issue. 1999. Vol.111. P.179–330.
13. *Jaume S.C., Sykes L.R.* Evolving towards a critical point: A review of accelerating seismic moment/Energy release prior to large and great earthquakes // Pure Appl. Geophys. 1999. Vol.155. P.279–306.
14. *Pepke G.F., Carlson J.M., Shaw B.E.* Prediction of large events on a dynamical model of fault // J. Geophys. Res. 1994. Vol.99. P.6769–6788.
15. *Kossobokov V.G., Carlson J.M.* Active zone size vs. activity: A study of different seismicity patterns in the context of the prediction algorithm M8 // J. Geophys. Res. 1995. Vol.100. P.6431–6441.
16. *Shebalin P., Zaliapin I., Keilis-Borok V.I.* Premonitory Rise Of The Earthquakes' Correlation Range: Lesser Antilles // Phys. Earth Planet. Inter. 2000. Vol.122. P.241–249.
17. *Gabrielov A.M., Zaliapin I.V., Newman W.I., Keilis-Borok V.I.* Colliding cascades model for earthquake prediction // Geophys. J. Int. 2000. Vol.143. P.427–437.
18. *Zöller G., Hainzl S., Kurths J.* Observation of growing correlation length as an indicator for critical point behavior prior to large earthquakes // J. Gephys. Res. 2001. Vol.106. P.2167–2176.

19. *Zöller G., Hainzl S.* Detecting premonitory seismicity patterns based on critical point dynamics // Natural Hazards and Earth System Sciences. 2001. Vol.1. P.93–98.
20. *Zaliapin I., Keilis-Borok V., Axen G.* Premonitory spreading of seismicity over the fault's network in S. California: precursor accord // J. Geoph. Res. 2002 (Accepted).
21. *Caputo M., Gasperini P., Keilis-Borok V.I., Marcelli L., Rotwain I.M.* Earthquakes' swarms as forerunners of strong earthquakes in Italy // Ann. Geofis. (Roma). 1977. Vol.30. P.269–283.
22. *Keilis-Borok V.I.* Earthquake prediction: State-of-the-art and emerging possibilities // Ann. Rev. Earth Planet. Sci. 2002. Vol.30. P.1–33.
23. *Keilis-Borok V.I., Kossobokov V.G.* Premonitory activation of earthquake flow: algorithm M8 // Phys. Earth Planet. Inter. 1990. Vol.61. P.73–83.
24. *Keilis-Borok V.I., Rotwain I.M.* Diagnosis of time of increased probability of strong earthquakes in different regions of the world: algorithm CN // Phys. Earth Planet. Inter. 1990. Vol.61. P.57–72.
25. *Vorobieva I.A.* Prediction of a subsequent large earthquake // Phys. Earth Planet. Inter. 1999. Vol.111. P.197–206.
26. *Molchan G.M., Dmitrieva O.E., Rotwain I.M., Dewey J.* Statistical analysis of the results of earthquake prediction, based on bursts of aftershocks // Phys. Earth Planet. Inter. 1990. Vol.61. P.128–139.
27. *Kossobokov V.G., Romashkova L.L., Keilis-Borok V.I., Healy J.H.* Testing earthquake prediction algorithms: Statistically significant real-time prediction of the largest earthquakes in the Circum-Pacific, 1992-1997 // Phys. Earth Planet. Inter. 1999. Vol.111, N 3-4. P.187–196.
28. *Varnes D.J.* Predicting earthquakes by analyzing accelerating precursory seismic activity // Pure Appl. Geophys. 1989. Vol.130. P.661–686.
29. *Bufe C.G., Varnes D.J.* Predictive modeling of the seismic cycle of the great San Francisco bay region // J. Geophys. Res. 1993. Vol.98. P.9871–9883.
30. *Bowman D.D., Ouillon G., Sammis C.G., Sornette A., Sornette D.* An observational test of the critical earthquake concept // J. Geophys. Res. 1998. Vol.103. P.24359–24372.
31. *Yamashita T., Knopoff L.* Model for intermediate-term precursory clustering of earthquakes // J. Geophys. Res. 1992. Vol.97. P.19,873–19,879.
32. *Lyakhovsky V., Ben-Zion Y., Agnon A.* Earthquake cycle, fault zones and seismicity patterns in a rheologically layered lithosphere // J. Geophys. Res. 2001. Vol.106. P.4103–4120.
33. *Soloviev A., Vorobieva I.* Long-range interaction between synthetic earthquakes in the model of block structure dynamics, fifth workshop on non-Linear dynamics and earthquake prediction, 4–22 October 1999. Trieste: ICTP, H4.SMR/1150-4. 18 p.
34. *Zaliapin I., Keilis-Borok V., Ghil M.* A boolean delay model of colliding cascades. II: prediction of critical transitions // J. Stat. Phys. 2001 (Submitted).
35. *Sadovsky M.A.* Randomness and instability in geophysical processes (In Russian) // Fizika Zemli. 1989. Vol.2. P.3–12.
36. *Knopoff L.* Self-organization and the development of pattern: Implications for earthquake prediction // Proc. Amer. Philosoph. Soc. 1993. Vol.137. P.339–349.
37. *Bak P.* How nature works: The science of self-organized criticality. N.Y.: Copernicus, 1996.
38. *Turcotte D.L.* Fractals and chaos in geology and geophysics. Cambridge University Press, 1997.
39. *Sornette D.* Critical phenomena in natural sciences. Chaos, fractals, self-organization and disorder: Concepts & Tools. Springer Ser. Synerg., Heidelberg. 2000. N.Y.: Springer-Verlag. P.432.

40. *Rundle B.J., Turcotte D.L., Klein W. Eds.* Geocomplexity and the physics of earthquakes. Washington, DC: AGU, 2000.
41. *Turcotte D.L., Newman W.I., Gabrielov A.* A statistical physics approach to earthquakes, geocomplexity and the physics of earthquakes. Washington: AGU, 2000.
42. *Kossobokov V.G., Keilis-Borok V.I., Turcotte D.L, Malamud B.D.* Implications of a statistical physics approach to earthquake hazard assessment and forecasting // Pure Appl. Geophys. 2002. Vol.157. P.2323–2349.
43. *Frohlich C., Davis S.D.* Single-link cluster analysis as a method to evaluate spatial and temporal properties of earthquake catalogues // Geophys. J. Int. 1990. Vol.100. P.19–32.
44. *Gelfand I.M., Guberman Sh.A., Keilis-Borok V.I., Knopoff L., Press F., Ranzman E.Ya., Rotwain I.M., Sadovsky A.M.* Pattern recognition applied to earthquake epicenters in California // Phys. Earth Planet. Inter. 1976. Vol.11. P.227–283.
45. *Molchan G.M.* Earthquake prediction as a decision-making problem // Pure Appl. Geophys. 1997. Vol.149. P.233–247.
46. *Blanter E.M., Shnirman M.G.* On multifractal theory approach to the clustering of epicenters // Comput. Seism. and Geodyn. AGU. 1992. Vol.2. P.37–45.
47. *Шаповал А.Б., Шнирман М.Г.* Сценарий сильных событий в модели накопления песка // Наст. сб.
48. *Keilis-Borok V.I., Knopoff L., Rotwain I.M.* Bursts of aftershocks, long-term precursors of strong earthquakes // Nature. 1980. Vol.283. P.259–263.
49. *Knopoff L., Levshina T., Keilis-Borok V.I., Mattoni C.* Increased long-range intermediate-magnitude earthquake activity prior to strong earthquakes in California // J. Geophys. Res. 1996. Vol.101. P.5779–5796.